

Beamforming and Resource Allocation for Delay Optimization in RIS-Assisted OFDM Systems

Yu Ma, Xiao Li, *Member, IEEE*, Chongtao Guo, *Member, IEEE*, Le Liang, *Member, IEEE*, Shi Jin, *Fellow, IEEE*

Abstract—This paper investigates a joint beamforming and resource allocation problem in downlink reconfigurable intelligent surface (RIS)-assisted orthogonal frequency division multiplexing (OFDM) systems to optimize average delay, where data packets for each user arrive at the base station stochastically. The sequential optimization problem is inherently a Markov decision process (MDP), thus falling within the scope of reinforcement learning. To effectively handle the mixed action space and reduce the state space dimensionality, a hybrid deep reinforcement learning (DRL) approach is proposed. Specifically, proximal policy optimization (PPO)- Θ is employed to optimize the RIS phase shift design, while PPO- N is responsible for subcarrier allocation decisions. The active beamforming at the base station is then derived from the jointly optimized RIS phase shifts and subcarrier allocation decisions. To further mitigate the curse of dimensionality associated with subcarrier allocation, a multi-agent strategy is introduced to optimize subcarrier allocation indicators more efficiently. Moreover, to achieve more adaptive resource allocation and accurately capture network dynamics, key factors closely related to average delay—such as the number of backlogged packets in buffers and current packet arrivals—are incorporated into the state space. Furthermore, a transfer learning framework is introduced to enhance training efficiency and accelerate convergence. Simulation results demonstrate that the proposed algorithm significantly reduces average delay, enhances resource allocation efficiency, and achieves superior system robustness and fairness compared to baseline methods.

Index Terms—Reconfigurable intelligent surface, deep reinforcement learning, OFDM, delay optimization.

I. INTRODUCTION

WITH the continuous evolution of wireless communication technologies, sixth-generation (6G) wireless communication systems are envisioned to achieve unprecedented performance in terms of capacity, latency, reliability, and energy efficiency [1]. To meet the stringent demands of future applications, extensive research is being conducted on enhancing the fundamental capabilities of wireless systems [2]. Among the various enabling technologies, reconfigurable intelligent surfaces (RIS) have emerged as a key enabler [3], drawing significant research interest due to their potential to reconfigure the wireless propagation environment and support enhanced system performance.

Yu Ma, Xiao Li, and Shi Jin are with the National Mobile Communications Research Laboratory, Southeast University, Nanjing 210096, China (e-mail: yuma@seu.edu.cn; li_xiao@seu.edu.cn; jinshi@seu.edu.cn).

Chongtao Guo is with the College of Electronics and Information Engineering, Shenzhen University, Shenzhen 518060, China (e-mail: ct-guo@szu.edu.cn).

Le Liang is with the National Mobile Communications Research Laboratory, Southeast University, Nanjing 210096, China, and also with the Purple Mountain Laboratories, Nanjing 211111, China (e-mail: lliang@seu.edu.cn).

As a critical performance metric, latency plays a vital role in determining the overall performance of wireless systems, particularly for mission-critical applications such as remote surgery, autonomous driving, factory automation, and intelligent transportation systems [4]. These applications often require real-time data exchange. In such scenarios, even a small increase in latency can lead to severe consequences, such as system failures, road accidents, or disrupted services. Therefore, ensuring ultra-low latency, often on the order of tens of milliseconds or less [5], is essential for numerous mission-critical applications in the 6G era.

However, given the inherently limited nature of wireless resources, ensuring low-latency communication in RIS-assisted wireless systems remains a fundamental challenge, where the phase design and resource allocation are coupled. In addition to the challenge caused by joint optimization of phase design and resource allocation, limited spectrum and power resources constrain the system's ability to support high data rates and real-time responsiveness, multi-path effects introduce rapid fluctuations in channel conditions and signal quality [6], which necessitates network management to be adaptive to the environment. On the other hand, different users may have different numbers of backlogged packets, which needs to be taken into account in delay-aware resource allocation [7]. Therefore, in delay-aware RIS-assisted wireless networks, it is critical to make sequential resource allocation and phase design decisions while being adaptive to real-time channel conditions and queue status [8], which is challenging due to complex network environment and mixed decision variables including continuous RIS phase shifts design and discrete subcarrier.

A. Prior Works and Motivation

The delay refers to the duration from the moment the packet is generated at the transmitter to its reception by the receiver. This metric is crucial for evaluating the performance of communication networks, especially for applications requiring real-time responsiveness. Numerous studies [9]–[11] have shown that queuing delay constitutes the dominant component of overall latency compared to other components, such as processing latency, transmission latency, and propagation latency.

To address delay-aware resource allocation, some works leverage large-scale fading for spectrum and power management. For instance, in device-to-device (D2D)-enabled vehicular networks, resource allocation based on large-scale fading improves vehicle-to-infrastructure (V2I) ergodic capacity while ensuring vehicle-to-vehicle (V2V) reliability [12].

Similarly, single-input multiple-output (SIMO) systems have adopted power and rate allocation strategies using average signal and interference statistics under reliability and energy efficiency constraints [13]. Sun *et al.* further proposed a resource block and power control algorithm for D2D-based V2V communications without relying on instantaneous channel state information (CSI) [14]. However, these static methods struggle to adapt to rapid channel variations. To address this, Lyapunov optimization has gained traction for real-time delay-aware resource management, accounting for queue dynamics, channel fluctuations, and system constraints. For example, Guo *et al.* developed a cross-layer Lyapunov framework combining transport-layer rate control and physical-layer allocation to meet delay targets [15]. Similar approaches have led to robust scheduling policies that ensure queue stability and service quality in dynamic environments [16]–[18].

Beyond conventional optimization techniques, deep reinforcement learning (DRL)-based algorithms have emerged as powerful tools for addressing delay-aware sequential resource allocation in wireless communication systems, offering a favorable balance between performance and computational complexity [19]. Leveraging the Markov decision process (MDP) framework, DRL is particularly well-suited for real-time, sequential resource allocation decisions. Early efforts in this domain, such as the Q-learning-based link scheduling algorithm proposed in [20], demonstrate how queue length, channel conditions, and energy constraints can be jointly considered to optimize average transmission delay. As the complexity of network environments increases, research has evolved from single-agent to multi-agent paradigms. For instance, multi-agent deep reinforcement learning (MADRL) has been adopted to better handle distributed decision-making scenarios. In [21], each V2V link is modeled as an autonomous agent that dynamically performs spectrum sharing and power control, effectively reducing latency while minimizing interference with V2I communications.

While RIS has enhanced spectral efficiency, coverage, and energy efficiency [22]–[26], its application in latency-sensitive scenarios remains limited. Most existing works focus on mobile edge computing and neglect queuing delay, which is crucial for real-time communication [27]–[29]. For instance, [27] minimized task delay and energy in RIS-assisted non-orthogonal multiple access networks, and [28] addressed joint delay and rate in multiple-input multiple-output mobile edge computing systems. To address this gap, recent studies adopt Lyapunov-based methods for queue-aware resource allocation, converting long-term delay goals into per-slot decisions to adapt to dynamic traffic [30], [31]. For example, [31] jointly optimized power, channel assignment, and reflection coefficients in a semi-grant-free RIS-assisted system, improving queue stability over RIS-free baselines. However, current approaches remain insufficient. Many rely on complex alternating optimization and fail to explicitly include queuing delay in the objective, limiting their effectiveness in truly delay-sensitive RIS-assisted systems.

This research aims to bridge this gap by proposing a novel approach that integrates RIS technology with advanced optimization methods, including DRL techniques, to optimize av-

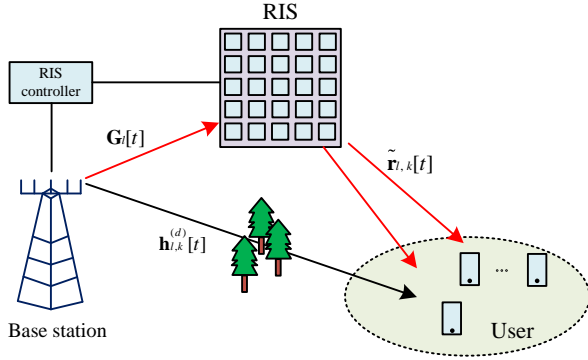
erage delay and enhance network performance. Our approach provides a new perspective on addressing latency challenges in RIS-assisted systems and offers a fresh direction for improving system performance in delay-sensitive applications. This work seeks to unlock the untapped potential of RIS in managing queuing delay in practical communication systems, ultimately enhancing the efficiency of RIS-assisted wireless networks.

B. Contributions and Organization

This paper aims to investigate resource allocation methods for delay optimization in RIS-assisted networks by leveraging DRL, with a particular focus on maintaining user fairness. To achieve this goal, a hybrid DRL framework is proposed to tackle the challenge of delay optimization in such networks. The main contributions of this work are summarized as follows.

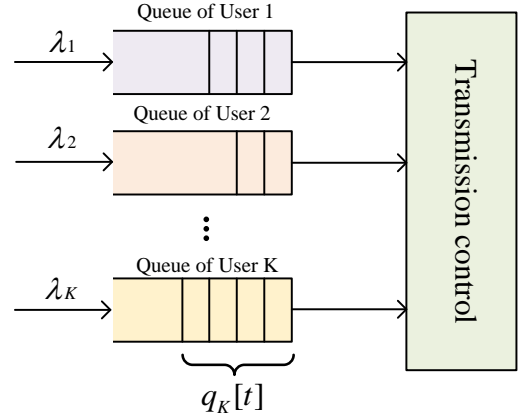
- A hybrid DRL framework is adopted, where the base station (BS) controller acts as the agent and is trained using proximal policy optimization (PPO). Specifically, PPO- Θ with continuous action space is used for RIS phase shift optimization, while PPO- N with discrete action space handles subcarrier allocation. To address the curse of dimensionality, a multi-agent strategy is employed, where each agent is responsible for the allocation of a single subcarrier.
- To ensure low delay, fairness, and adaptability, the state space incorporates CSI, the number of arriving packets, and the number of backlogged packets in each buffer. This enables the agent to capture both channel conditions and delay status for more efficient resource allocation in dynamic environments.
- We leverage transfer learning to overcome slow convergence during the initial stage, which arises from weak incentives in the direct delay-aware reward design. Specifically, we first train the agent with the objective of maximizing the minimum rate. Once a certain performance level is achieved, the pre-trained PPO- Θ is loaded as the initial model and further trained using the reward function and algorithm proposed in this work.
- We evaluate the proposed method across various RIS-assisted communication network configurations, demonstrating its superiority over baseline methods. Simulation results indicate that the method significantly reduces average delay while ensuring user fairness, demonstrating its superiority over baseline methods. Specifically, fairness is enhanced in the balanced accumulation of data packets across user buffers, even under varying arrival rates. Moreover, the method exhibits excellent robustness, as it maintains stable performance under different delay taps, user distributions, and Rician fading factors.

The rest of the paper is organized as follows. In Section II, the system model is introduced, followed by the formulation of the joint RIS phase and resource allocation optimization problem. At the end of this section, the optimization problem is formally defined. In Section III elaborates our proposed hybrid DRL-based scheme, including the overall framework, PPO- Θ design, PPO- N design, beamforming design, and



(a) Illustration of a RIS-assisted OFDM-MISO system communication scenario.

Fig. 1. System model.



(b) Queuing model at the base station.

training methodology. Section IV presents numerical simulations and complexity analysis to validate the proposed method. Finally, conclusions are presented in Section V.

C. Notations

Scalar variables are denoted by normal-face letters x , while vectors and matrices are denoted by lower and upper case letters, \mathbf{x} and \mathbf{X} , respectively. The sets of complex and real numbers are denoted by \mathbb{C} and \mathbb{R} , respectively. Superscripts $(\cdot)^T$, $(\cdot)^*$, and $(\cdot)^H$ represent the transpose, conjugate, and conjugate transpose operations of a matrix, respectively. The notation $\|\cdot\|$ represents the ℓ_2 norm of a vector. The expectation operator is denoted as $\mathbb{E}[\cdot]$. The notation $\text{diag}(\cdot)$ indicates a diagonal matrix construed by the entries of the input vector. The notation $\mathcal{CN}(\mu, \sigma^2)$ is used to denote a circularly symmetric complex Gaussian distribution with mean $(\cdot)^+$ refers to $\max(\cdot, 0)$.

II. SYSTEM MODEL AND PROBLEM FORMULATION

We consider an RIS-assisted downlink multiple-input single-output (MISO) orthogonal frequency division multiplexing (OFDM) communication system, as illustrated in Fig. 1(a), where a BS equipped with N_t antennas serves K single-antenna users. An RIS comprising M passive reflecting elements is deployed to effectively enhance the transmission quality. The entire communication duration is divided into T_{sum} timeslots, indexed by $\{1, 2, \dots, t, \dots, T_{\text{sum}}\}$, each with a fixed length of T . Within each time slot, the wireless channel is assumed to remain approximately static. Each user's data packets, which arrive randomly at the corresponding buffer at the BS, follow a first-come, first-served (FCFS) discipline, as illustrated in Fig. 1(b). In each time slot, the accumulated packets in the buffer k are scheduled for transmission to the user k . Packets that can not be delivered will remain in the buffer and continue to accumulate, resulting in increased packet delay over time.

A. Signal Model

In the MISO-OFDM system considered in this paper, $\tilde{\mathbf{h}}_{l,k}^{(d)}[t] \in \mathbb{C}^{1 \times N_t}$, $l = 0, 1, \dots, L_0 - 1$ represents the time-domain baseband equivalent channel of the direct link from the BS to the user k at the time slot t , where L_0 denotes the number of tap delays. Similarly, $\tilde{\mathbf{G}}_l[t] \in \mathbb{C}^{M \times N_t}$, $l = 0, 1, \dots, L_1 - 1$ and $\tilde{\mathbf{r}}_{l,k}[t] \in \mathbb{C}^{1 \times M}$, $l = 0, 1, \dots, L_2 - 1$ respectively denote the time-domain baseband equivalent channels from the BS to the RIS and from the RIS to the user k at the time slot t , where L_1 and L_2 are their respective numbers of tap delays. Therefore, the total maximum number of delay taps is $L = \max\{L_0, L_1 + L_2 - 1\}$. Thus, the overall channel from the BS to the user k at the time slot t can be expressed as

$$\begin{aligned} \tilde{\mathbf{h}}_{l,k}[t] &= \tilde{\mathbf{h}}_{l,k}^{(d)}[t] + \sum_{i=0}^{L_2-1} \tilde{\mathbf{r}}_{i,k}[t] \Phi[t] \tilde{\mathbf{G}}_{l-i}[t] \\ &= \tilde{\mathbf{h}}_{l,k}^{(d)}[t] + \sum_{i=0}^{L_2-1} \varphi[t]^T \text{diag}(\tilde{\mathbf{r}}_{i,k}[t]) \tilde{\mathbf{G}}_{l-i}[t] \\ &= \tilde{\mathbf{h}}_{l,k}^{(d)}[t] + \varphi[t]^T \sum_{i=0}^{L_2-1} \text{diag}(\tilde{\mathbf{r}}_{i,k}[t]) \tilde{\mathbf{G}}_{l-i}[t], \\ & \quad l = 0, 1, \dots, L - 1, \end{aligned} \quad (1)$$

where $\tilde{\mathbf{G}}_l[t] = \mathbf{0}$, $l \in \{1 - L_2, \dots, -1\} \cup \{L_1, \dots, L - 1\}$, and $\Phi[t] = \text{diag}(e^{j\theta_1[t]}, e^{j\theta_2[t]}, \dots, e^{j\theta_M[t]}) \in \mathbb{C}^{M \times M}$ is the RIS reflection phase shifts matrix at the time slot t . Let $\varphi[t] = [e^{j\theta_1[t]}, e^{j\theta_2[t]}, \dots, e^{j\theta_M[t]}]^T \in \mathbb{C}^{M \times 1}$ denote the RIS reflection phase shifts vector at the time slot t , where $\theta_m[t]$ refers to the phase shift of the reflection element m at the time slot t . We set $\tilde{\mathbf{h}}_{l,k}^{(r)}[t] = \sum_{i=0}^{L_2-1} \text{diag}(\tilde{\mathbf{r}}_{i,k}[t]) \tilde{\mathbf{G}}_{l-i}[t]$, thus $\tilde{\mathbf{h}}_{l,k}[t]$ can further be expressed as

$$\tilde{\mathbf{h}}_{l,k}[t] = \tilde{\mathbf{h}}_{l,k}^{(d)}[t] + \varphi[t]^T \tilde{\mathbf{h}}_{l,k}^{(r)}[t]. \quad (2)$$

To leverage the advantages of OFDM, we assume that the length of the cyclic prefix exceeds the maximum delay taps,

i.e., $N_{CP} \geq L$. This ensures that inter-symbol interference is eliminated. Furthermore, the discrete Fourier transform (DFT) is applied to transform the time-domain channel into the frequency-domain channel, which can be expressed as

$$\begin{aligned} \bar{\mathbf{h}}_{n,k}[t] &= \sum_{l=0}^{L-1} \tilde{\mathbf{h}}_{l,k}[t] e^{-\frac{j2\pi ln}{N}} \\ &= \sum_{l=0}^{L_0-1} \tilde{\mathbf{h}}_{l,k}^{(d)}[t] e^{-\frac{j2\pi ln}{N}} + \boldsymbol{\varphi}[t]^T \sum_{l=0}^{L_1+L_2-2} \tilde{\mathbf{h}}_{l,k}^{(r)}[t] e^{-\frac{j2\pi ln}{N}} \\ &= \bar{\mathbf{h}}_{n,k}^{(d)}[t] + \boldsymbol{\varphi}[t]^T \bar{\mathbf{h}}_{n,k}^{(r)}[t], \end{aligned} \quad (3)$$

where $\bar{\mathbf{h}}_{n,k}^{(d)}[t]$ and $\bar{\mathbf{h}}_{n,k}^{(r)}[t]$ represent the direct link channel and cascaded reflection channel of the user k on subcarrier n at the time slot t in the frequency domain, respectively. Therefore the received signal of the user k on subcarrier n at the time slot t can be represented as

$$y_{n,k}[t] = (\bar{\mathbf{h}}_{n,k}^{(d)}[t] + \boldsymbol{\varphi}[t]^T \bar{\mathbf{h}}_{n,k}^{(r)}[t]) \mathbf{w}_n[t] s_n[t] + \nu_n[t], \quad (4)$$

where $\mathbf{w}_n[t] \in \mathbb{C}^{N_t \times 1}$ denotes the beamforming vector on subcarrier n at the time slot t , $s_n[t]$ represents the transmitted signal on subcarrier n at the time slot t with $\mathbb{E}\{|s_n[t]|^2\} = 1$, and $\nu_n[t]$ is additive Gaussian white noise, which satisfies $\nu_n[t] \sim \mathcal{CN}(0, \sigma^2)$. Thus, the signal-to-noise ratio (SNR) of the user k on subcarrier n at the time slot t can be expressed as

$$\gamma_{n,k}[t] = \frac{|(\bar{\mathbf{h}}_{n,k}^{(d)}[t] + \boldsymbol{\varphi}[t]^T \bar{\mathbf{h}}_{n,k}^{(r)}[t]) \mathbf{w}_n[t]|^2}{\sigma^2}. \quad (5)$$

Therefore, the achievable rate for the user k at the time slot t is given by

$$R_k[t] = W \sum_{n=1}^N \alpha_{n,k}[t] \log_2(1 + \gamma_{n,k}[t]), \quad (6)$$

where W represents the bandwidth of the subcarrier, and $\alpha_{n,k}[t]$ denotes the subcarrier allocation indicator at the time slot t . In particular, we have $\alpha_{n,k}[t] = 1$ if subcarrier n is allocated to the user k at the time slot t , and $\alpha_{n,k}[t] = 0$ otherwise.

B. Queueing Model

In practice, packets arrive randomly at the transmitter and stored provisionally in a buffer before transmission to the receiver. Following the recommendation of the 3rd generation partnership project (3GPP), we model the packet arrival process as a Poisson process [32]. Specifically, the number of packets arriving at the buffer k during time slot t , denoted by $\ell_k[t]$, follows the probability density function

$$\Pr\{\ell_k[t] = i\} = \frac{(\lambda_k T)^i}{i!} e^{-\lambda_k T}, \quad (7)$$

where λ_k is the average packet arrival rate of the user k . The number of packets that can be theoretically transmitted from

the buffer k to the user k in the time slot t is denoted as $D_k[t]$ given by

$$D_k[t] = \left\lfloor \frac{TR_k[t]}{L} \right\rfloor, \quad (8)$$

where $\lfloor \cdot \rfloor$ is the floor operation and L is the number of bits contained in a packet. However, the number of packets that are eventually delivered during slot t , denoted by $\Xi_k[t]$, is bounded by the number of accumulated packets in the buffer k , as given by

$$\Xi_k[t] = \min\{D_k[t], q_k[t]\}, \quad (9)$$

where $q_k[t]$ denotes the number of backlogged packets in the buffer k at the beginning of time slot t . Thus, the queue in the buffer k updates according to

$$q_k[t+1] = q_k[t] + \ell_k[t] - \Xi_k[t]. \quad (10)$$

C. Problem Formulation

The delay experienced by each packet consists of two components: queueing delay and transmission delay, both of which are affected by the subcarrier allocation indicator, the RIS reflection phase shift, and the beamforming vector at the base station. Therefore, both delay components are considered in this paper. Let $m(k)$ represent the number of packets successfully delivered to the user k during the communication period with T_{sum} timeslots. The delay of the g -th packet of the user k during the considered time duration is denoted as $T_D^{(k)}(g)$ for all $g \in \{1, 2, \dots, m(k)\}$, which accounts for both queueing and transmission delays.

In this paper, our objective is to minimize the average delay by jointly optimizing the subcarrier allocation shift $\alpha_{n,k}[t]$, beamforming vectors at the BS $\mathbf{w}_n[t]$, and RIS reflection phase shifts $\theta_m[t]$. Specifically, the problem is formulated as

$$\begin{aligned} \min_{\{\theta_m[t], \alpha_{n,k}[t], \mathbf{w}_n[t]\}} & \frac{1}{K} \sum_{k=1}^K \frac{1}{m(k)} \sum_{g=1}^{m(k)} T_D^{(k)}(g) \\ \text{s.t.} & \alpha_{n,k}[t] \in \{0, 1\}, \quad \forall n, k, t, \end{aligned} \quad (11a)$$

$$\sum_{k=1}^K \alpha_{n,k}[t] \leq 1, \quad \forall n, t, \quad (11b)$$

$$\sum_{n=1}^N \|\mathbf{w}_n[t]\|^2 \leq P_{\max}, \quad \forall t, \quad (11c)$$

$$\theta_m[t] \in [0, 2\pi], \quad \forall m, t, \quad (11d)$$

where (11a) describes the binary constraints of the subcarrier allocation indicators, (11b) demonstrates that each subcarrier can be allocated to at most one user, (11c) ensures that the total power consumption of the BS does not exceed its maximum budget P_{\max} , and (11d) limits each RIS element's reflection phase shift to its allowable range.

III. DEEP REINFORCEMENT LEARNING BASED ALGORITHM

This section introduces a DRL-based framework for addressing the problem in (11), highlighting the core design principles, the corresponding training methodology and the computational complexity of proposed algorithm.

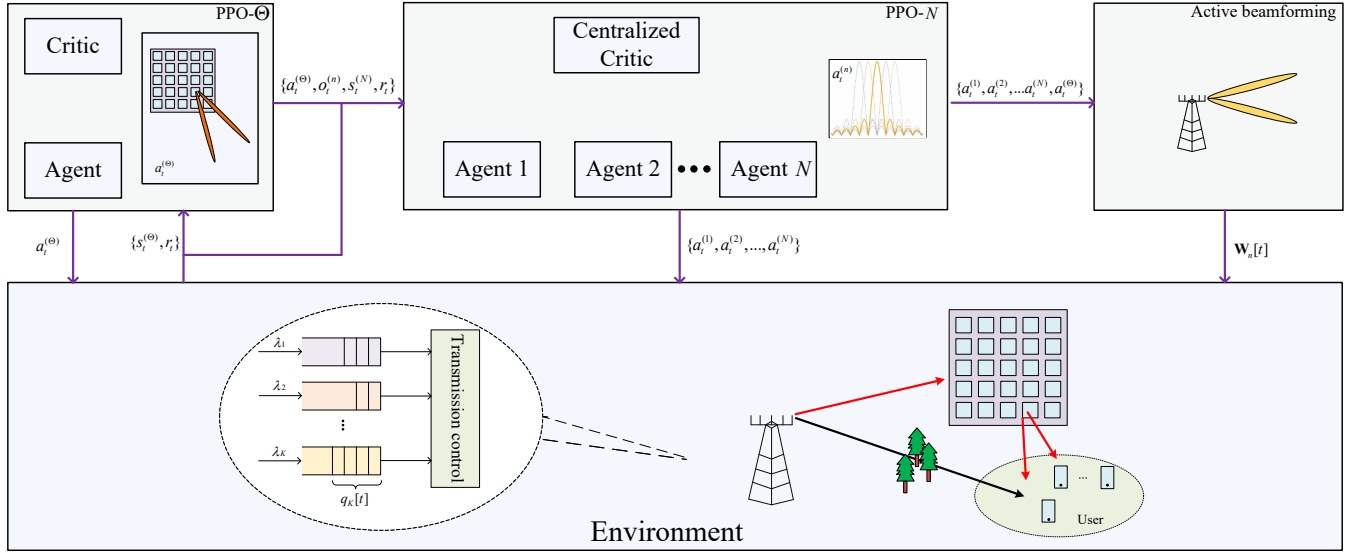


Fig. 2. Structure of the proposed DRL framework.

A. Overall Framework

The optimization problem presented in equation (11) necessitates determining the RIS phase shifts and resource allocation for each time slot, where decisions made in the current slot directly influence the number of packets that can be delivered, thereby affecting the queue length in the subsequent slot. Therefore, the problem (11) is a sequential decision making issue, which can be typically characterized by MDP. To this end, a hybrid RL approach is adopted, wherein a central controller collects information regarding the channel state information and the states of all buffers. The central controller, deployed at the BS, functions as an agent responsible for controlling the RIS and subcarrier allocation. It explores the unknown communication environment to acquire experience, which is subsequently utilized to guide policy design and optimize the RIS reflection phase shift and subcarrier allocation strategies based on observations of the environment state. Specifically, the PPO- Θ is utilized to predict the RIS reflection phase shift, while PPO- N is applied to determine the subcarrier allocation indicators. The detailed algorithm framework is illustrated in Fig. 2.

B. PPO- Θ Design

The PPO- Θ model is employed to optimize the RIS reflection phase shift. Given the continuous nature of RIS phase shifts, the PPO algorithm is utilized to train an agent comprising an actor network for action selection and a critic network for state value estimation. Specifically, the actor network determines the RIS reflection phase shift, while the critic network evaluates the effectiveness of the selected policy. In the following, we introduce the state, action, and reward, which are the three fundamental elements for reinforcement learning algorithm design.

In wireless communication, channel state information significantly impacts communication performance, making it es-

Algorithm 1 DRL-based Resource Allocation Algorithm

Input: $\bar{\mathbf{h}}_{n,k}^{(d)}[t]$, $\bar{\mathbf{h}}_{n,k}^{(r)}[t]$, $q_k[t]$, and $\ell_k[t]$.

Output: $\theta_m[t]$, $\alpha_{n,k}[t]$ and $\mathbf{w}_n[t]$.

- 1: Initialize network parameters $\theta^{(\Theta)}$, $\phi^{(\Theta)}$, $\theta^{(N)}$, $\phi^{(N)}$.
- 2: **for** each episode **do**
- 3: Initialize buffers.
- 4: Collect $\bar{\mathbf{h}}_{n,k}^{(d)}[t]$, $\bar{\mathbf{h}}_{n,k}^{(r)}[t]$, $q_k[t]$, $R_k[t-1]$ and $\ell_k[t]$.
- 5: Packets arrive at buffers.
- 6: **for** time step $t \in [1, T_{\text{sum}}]$ **do**
- 7: Obtain action $\theta_m[t]$ from PPO- Θ .
- 8: Calculate the equivalent channel $\mathbf{h}_{n,k}^{\text{eff}}$.
- 9: Obtain action $\alpha_{n,k}[t]$ from PPO- N .
- 10: Calculate $\mathbf{w}_n[t]$ according Section III-D.
- 11: Transmit packets.
- 12: Packets arrive at buffers.
- 13: Update buffers of each user.
- 14: Calculate the reward and obtain new state.
- 15: Save the experience to the replay buffer 1 and replay buffer 2.
- 16: **end for**
- 17: **for** agent update times $n \in [1, K_{\text{update}}]$ **do**
- 18: Sample data from replay buffer 1 and update PPO- Θ .
- 19: Sample data from replay buffer 2 and update PPO- N .
- 20: **end for**
- 21: **end for**

sential for RIS reflection phase shift design and subcarrier allocation. Moreover, the buffer state information, i.e., the number of queuing packets of each user, and factors that may influence the buffer state, including the number of current arrival packets, need to be observed every slot to make sequential delay-aware decision. Therefore, the environment

state $s_t^{(\Theta)}$ is defined as the channel state information at the time slot t , including the direct link channel $\bar{\mathbf{h}}_{n,k}^{(d)}[t]$ and cascaded reflection channel $\bar{\mathbf{h}}_{n,k}^{(r)}[t]$, the number of packets backlogged in each user's buffer $q_k[t]$, and the number of current arrival packets $\ell_k[t]$.

In reinforcement learning, an action refers to the decision or operation made by an agent in response to a given state of the environment. In the proposed framework, the action of PPO- Θ , denoted as $a_t^{(\Theta)}$, is defined as the RIS reflection phase shift vector $\Theta[t] = \{\theta_1[t], \theta_2[t], \dots, \theta_M[t]\}$.

The reward function plays a pivotal role in DRL, as it directly steers the agent's learning behavior toward the desired optimization objective. To effectively minimize the average delay in the system, it is essential to align the reward function with the optimization goal. To this end, the proposed framework defines the reward at each time step as the negative total number of packets queued in all users' buffers, formulated as

$$r_t = - \sum_{k=1}^K q_k[t], \quad (12)$$

This metric effectively captures the instantaneous queuing state of the network and provides an indirect yet meaningful proxy for overall transmission delay. From a packet-level perspective, if a packet is not transmitted upon arrival, it accumulates delay for each additional time slot as long as it remains in the buffer. Thus, the summation of queue length over all time steps reflects the aggregate queuing delay in the system. By maximizing the expected return under this reward formulation, the agent is naturally driven to reduce buffer backlogs and equivalently minimize the average delay of all users [33].

At the same time, to ensure effective policy learning and value estimation, the actor and critic networks in PPO- Θ are carefully designed with tailored neural architectures, as illustrated in Fig. 3(a).

a) Actor network design: The input to the actor network corresponds to the state observation $s_t^{(\Theta)}$, which includes both the direct channel $\bar{\mathbf{h}}_{n,k}^{(d)}[t]$ and the cascaded channel $\bar{\mathbf{h}}_{n,k}^{(r)}[t]$, with dimensions of $K \times N \times N_t$ and $K \times N \times M \times N_t$, respectively. Since neural networks cannot directly process complex-valued inputs, each complex channel element is decomposed into its real and imaginary parts. The resulting tensors are reshaped and combined to construct a $2K$ -channel input tensor $T_c^{(\Theta)}$ of size $NN_t \times (M+1)$, where the channels correspond to the real and imaginary components of the direct and cascaded channels for each user. This tensor is then processed by a convolutional neural network (CNN) to extract spatial features that characterize the wireless environment. The high-level channel representation extracted by the CNN is subsequently concatenated with the queue length $q_k[t]$ and the transmission power level $\ell_k[t]$, forming a one-dimensional feature vector. This vector is fed into a series of fully connected (FC) layers, which output the parameters of the action probability distribution. Finally, the RIS reflection phase shift action is sampled from this distribution.

b) Critic network design: The critic network adopts the same input structure and feature extraction architecture as

those of the actor network. However, it differs in its final layer, which is tailored to output a scalar value estimating the state value $V_{\phi^{(\Theta)}}(s_t^{(\Theta)}) \in \mathbb{R}$.

The policy objective function in PPO- Θ is employed to optimize the actor network and is defined as

$$\mathcal{J}(\theta^{(\Theta)}) = \mathbb{E}_t \left[\min(\bar{r}_t^{(\Theta)}(\theta^{(\Theta)}) \hat{A}_t^{(\Theta)}, \text{clip}(\bar{r}_t^{(\Theta)}(\theta^{(\Theta)}), 1 - \epsilon^{(\Theta)}, 1 + \epsilon^{(\Theta)}) \hat{A}_t^{(\Theta)}) \right] \quad (13)$$

where $\bar{r}_t^{(\Theta)}(\theta^{(\Theta)}) = \frac{\pi_{\theta^{(\Theta)}}(a_t^{(\Theta)}|s_t^{(\Theta)})}{\pi_{\theta_{\text{old}}^{(\Theta)}}(a_t^{(\Theta)}|s_t^{(\Theta)})}$ denotes the probability ratio between the new and old policies, $\epsilon^{(\Theta)}$ is a clipping factor used in PPO to stabilize learning by preventing excessively large changes of policy update, and $\hat{A}_t^{(\Theta)}$ is the generalized advantage estimation (GAE). The GAE can be computed by

$$\hat{A}_t^{(\Theta)} = \sum_{l=0}^{\infty} (\gamma\lambda)^l \delta_{t+l}^{(\Theta)}, \quad (14)$$

where γ is the discount factor, λ is the GAE parameter, and the temporal difference (TD) error $\delta_t^{(\Theta)}$ is defined by

$$\delta_t^{(\Theta)} = r_t + \gamma V_{\phi^{(\Theta)}}(s_{t+1}^{(\Theta)}) - V_{\phi^{(\Theta)}}(s_t^{(\Theta)}). \quad (15)$$

The critic network, parameterized by $\phi^{(\Theta)}$, is optimized by minimizing the following mean squared error loss

$$\mathcal{L}(\phi^{(\Theta)}) = \mathbb{E}_t \left[\left(r_t + \gamma V_{\phi^{(\Theta)}}(s_{t+1}^{(\Theta)}) - V_{\phi^{(\Theta)}}(s_t^{(\Theta)}) \right)^2 \right], \quad (16)$$

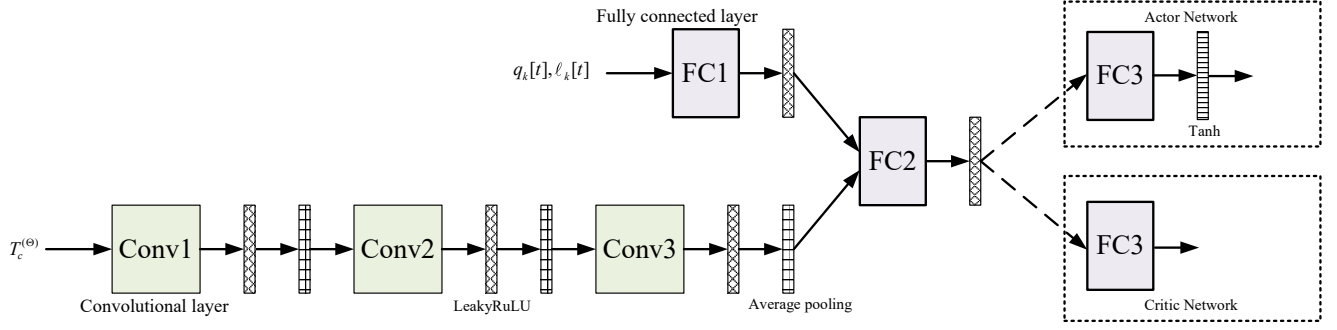
where $V_{\phi^{(\Theta)}}(s_{t+1}^{(\Theta)})$ and $V_{\phi^{(\Theta)}}(s_t^{(\Theta)})$ represent the value estimations of the next and current states, respectively.

C. PPO- N Design

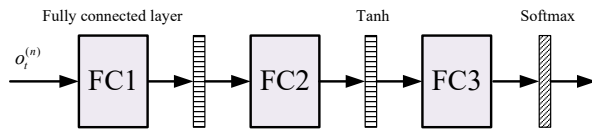
The PPO- N framework optimizes discrete subcarrier allocation indicators using a discrete PPO algorithm. A single-agent approach faces a huge action space of size K^N when allocating N subcarriers to K users, causing the curse of dimensionality. To address this, a multi-agent approach is used, where each of the N agents controls one subcarrier's allocation with an action space of size K , greatly reducing complexity. This design also naturally satisfies constraints (11a) and (11b).

Next, we present the definitions of the global state used by the critic network, the observation state observed by the agents, the reward, and the action.

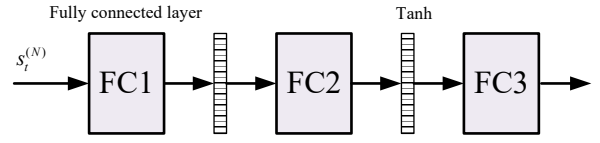
The global state $s_t^{(N)}$ used by the centralized critic includes the complete equivalent channel state information $\mathbf{h}_{n,k}^{\text{eff}}$ for all users and subcarriers, along with the global buffer state $q_k[t]$ and packet arrivals $\ell_k[t]$, enabling joint policy evaluation across agents. To reduce input dimensionality, $\mathbf{h}_{n,k}^{\text{eff}}$ is defined as $\bar{\mathbf{h}}_{n,k}^{(d)} + \varphi^T \bar{\mathbf{h}}_{n,k}^{(r)}$, where $\varphi[t]$ is the RIS reflection phase shifts vector generated by PPO- Θ . The local observation $o_t^{(n)}$ of agent n comprises the equivalent channel state from the BS to users on subcarrier n , buffer length $q_k[t]$, and packet arrivals $\ell_k[t]$.



(a) Actor and critic network architectures of PPO- Θ . While the figure illustrates the structurally similar components of the actor and critic networks in a unified manner for clarity, the two networks are implemented with separate parameters.



(b) Actor network architecture of PPO- N



(c) Centralized critic network architecture of PPO- N

Fig. 3. Network architecture.

Since the objective is to minimize average delay by jointly optimizing RIS phase shifts and subcarrier allocation, PPO- N and PPO- Θ share the reward function defined in (12). Since N agents are used to allocate N subcarriers, and each subcarrier has K possible allocation options, the action space $a_t^{(n)}$ of each agent is defined as $\{1, 2, \dots, K\}$.

At the same time, to ensure effective policy learning and value estimation, the actor and critic networks in PPO- N are carefully designed with tailored neural architectures, as described below.

a) Actor network design: The input to the actor network corresponds to each observation space $o_t^{(n)}$. This input is fed into a series of fully connected layers to generate the parameters of the action probability distribution, from which the action is sampled accordingly. The detailed architecture of the actor network is illustrated in Fig. 3(b).

b) Centralized critic network design: The input to the centralized critic network corresponds to the global state space $s_t^{(N)}$. This input is fed into a fully connected neural network to estimate the value of the global state. The critic network outputs a scalar value $V_{\phi^{(N)}}(s_t^{(N)})$, which approximates the expected return under the current policy. The detailed architecture of the critic network is illustrated in Fig. 3(c).

In the discrete action space setting, the policy loss function is modified accordingly

$$\mathcal{J}(\theta^{(n)}) = \mathbb{E} \left[\min \left(\bar{r}_t(\theta^{(n)}) \hat{A}_t^{(n)}, \text{clip}(\bar{r}_t(\theta^{(n)}), 1 - \epsilon^{(n)}, 1 + \epsilon^{(n)}) \hat{A}_t^{(n)} \right) \right] \quad (17)$$

where $\epsilon^{(n)}$ is a clipping factor, and $\bar{r}_t(\theta^{(n)})$ is the probability

ratio for agent n , given by

$$\bar{r}_t^{(n)}(\theta^{(n)}) = \frac{\pi_{\theta^{(n)}}(a_t^{(n)} | o_t^{(n)})}{\pi_{\theta_{\text{old}}^{(n)}}(a_t^{(n)} | o_t^{(n)})}. \quad (18)$$

$\hat{A}_t^{(n)}$ is the GAE for agent n , which is computed as

$$\hat{A}_t^{(n)} = \sum_{l=0}^{\infty} (\gamma \lambda)^l \delta_{t+l}^{(n)}, \quad (19)$$

where γ is the discount factor, λ is the GAE parameter, and the TD error is defined by

$$\delta_t^{(n)} = r_t + \gamma V_{\phi^{(N)}}(s_{t+1}^{(N)}) - V_{\phi^{(N)}}(s_t^{(N)}). \quad (20)$$

The value function for each agent is optimized by minimizing the following mean squared error loss

$$\mathcal{L}(\phi^{(N)}) = \mathbb{E}_t \left[\left(r_t^{(n)} + V_{\phi^{(N)}}(s_{t+1}^{(N)}) - V_{\phi^{(N)}}(s_t^{(N)}) \right)^2 \right], \quad (21)$$

where $V_{\phi^{(N)}}(s_{t+1}^{(N)})$ and $V_{\phi^{(N)}}(s_t^{(N)})$ represent the value estimations of the next and current global states, respectively, and $r_t^{(n)}$ denotes the reward obtained by agent n from subcarrier allocation decisions.

D. Active Beamforming Design

With the RIS reflection shift and subcarrier allocation indicator produced by PPO- Θ and PPO- N , the BS beamforming vectors $\mathbf{w}_n[t]$ for subcarrier n at the time slot t can be derived as maximum ratio transmission (MRT) in conjunction with the water-filling algorithm, i.e.,

$$\mathbf{w}_n[t] = \sqrt{p_n[t]} \bar{\mathbf{w}}_n[t], \quad (22)$$

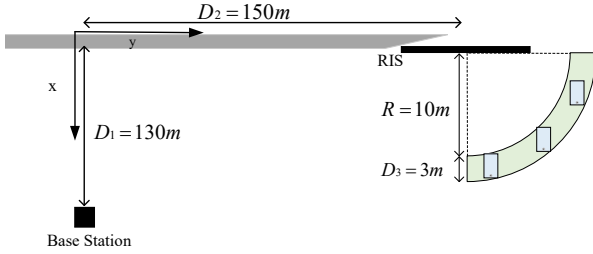


Fig. 4. Illustration of the simulated scenario.

where $\bar{\mathbf{w}}_{n,q}$ represents the optimal unit-norm beamforming vector and $p_n[t]$ refers to the transmission power on subcarrier n at the time slot t . In particular, $\bar{\mathbf{w}}_{n,q}$ can be expressed as,

$$\bar{\mathbf{w}}_n[t] = \frac{(\bar{\mathbf{h}}_{n,k}^{(d)}[t] + \boldsymbol{\varphi}[t]^T \bar{\mathbf{h}}_{n,k}^{(r)}[t])^H}{\|(\bar{\mathbf{h}}_{n,k}^{(d)}[t] + \boldsymbol{\varphi}[t]^T \bar{\mathbf{h}}_{n,k}^{(r)}[t])\|}, \forall n, t. \quad (23)$$

The $p_n[t]$ can be expressed by the following equation,

$$p_n[t] = \left(\frac{1}{\tau[t]} - \frac{1}{c_n[t]} \right)^+, \forall n, t, \quad (24)$$

where $c_n[t] = \frac{\|(\bar{\mathbf{h}}_{n,k}^{(d)}[t] + \boldsymbol{\varphi}[t]^T \bar{\mathbf{h}}_{n,k}^{(r)}[t])\|^2}{\sigma^2}$, and $\tau[t]$ is the Lagrange multiplier satisfying,

$$\sum_{n=1}^N \left(\frac{1}{\tau[t]} - \frac{1}{c_n[t]} \right)^+ = P_{\max}, \forall t. \quad (25)$$

E. Training

Since the RIS phase has not been optimized in the early stages of training, the system experiences low data rates and overall instability. As a result, the reward value decreases as the time step increases within an episode, making training difficult. To address this, this paper proposes a novel transfer reinforcement learning strategy. Specifically, in the initial training phase, the reward is set to $\min R_k[t]$, while the training process still follows Algorithm 1. The trained PPO- Θ model parameters are then saved and reloaded into Algorithm 1 as the new PPO- Θ model initialization parameters. The reward is then switched to (12), and training continues until convergence through continuous iterative optimization.

F. Computational Complexity

The computational complexity of PPO- Θ is $\mathcal{O}(KNN_t(2M+1))$, while that of PPO- N is $\mathcal{O}(KNN_t)$. On the other hand, the active beamforming operation incurs a complexity of $\mathcal{O}(NMN_t + N)$. As a result, the overall computational complexity of the proposed algorithm is $\mathcal{O}(KNN_t(2M+1) + KNN_t + NMN_t + N)$.

IV. NUMERICAL RESULTS

In this section, a comprehensive evaluation of the performance of the proposed DRL-based algorithm is conducted. Various simulation scenarios and baseline comparisons are considered to demonstrate its effectiveness in optimizing system performance.

 TABLE I
HYPER-PARAMETERS

Parameter	Value
Number of training episodes	300
PPO- Θ replay buffer size	1000
PPO- N replay buffer size	1000
PPO- Θ batch size	64
PPO- N batch size	64
Sample reuse K_{update}	10
PPO- Θ and PPO- N discount factor	0.9
PPO- Θ and PPO- N GAE parameter	0.95
PPO- Θ and PPO- N clip parameter	0.2
PPO- Θ and PPO- N entropy indicator	0.01
Learning rate of all actor networks	3×10^{-5}
Learning rate of all critic networks	5×10^{-5}

A. Simulation Settings

In this simulation, as illustrated in Fig. 4, a downlink MISO-OFDM system with three single-antenna users is considered, where the users are located in an annular region with inner and outer radii of 10 and 13 meters, respectively, within a 90-degree sector. The vertical and horizontal distances between the BS and the RIS are set to $D_1 = 150$ m and $D_2 = 130$ m, respectively. The number of reflecting elements on the RIS is $M = 64$, and the BS is equipped with 4 antennas. Furthermore, we assume a noise power spectral density of -174 dBm/Hz, a transmit power P_{\max} of 10 dBm, and a subcarrier bandwidth of 180 kHz. The distance between two adjacent antennas on the BS and between adjacent reflecting elements on the RIS is set to half a wavelength. The delay taps are set to $L_0 = 4$, $L_1 = 2$, and $L_2 = 3$, respectively. Additionally, for the direct BS-user link, Rayleigh fading channels are assumed, while Rician fading is considered for the reflection channels from BS to RIS and from RIS to users. The first tap of each channel is set as the line-of-sight (LoS) path, and the taps are non-line-of-sight (NLoS) paths. The Rician factors for the BS-RIS link and RIS-User link are respectively represented by

$$k_{\text{BR}} = \frac{P_{\text{LoS, BR}}}{P_{\text{NLoS, BR}}}, \quad k_{\text{RU}} = \frac{P_{\text{LoS, RU}}}{P_{\text{NLoS, RU}}}, \quad (26)$$

where, $P_{\text{LoS, BR}}$, $P_{\text{NLoS, BR}}$, $P_{\text{LoS, RU}}$, and $P_{\text{NLoS, RU}}$ represent the power of the LoS and NLoS paths for the respective links. In this simulation, $k_{\text{BR}} = 4$ dB and $k_{\text{RU}} = 5$ dB are assumed. The large-scale fading is defined as $\beta = \beta_0 \left(\frac{d}{d_0} \right)^{-\xi}$, where $\beta_0 = -30$ dB, $d_0 = 1$ m, d represents the link distance, and ξ is the path loss exponent. The path loss exponents for the BS-User link, BS-RIS link, and RIS-User link are $\xi_0 = 3.8$, $\xi_1 = 2.2$, and $\xi_2 = 2.4$, respectively.

The packet capacity L is set to 512 bits. In each episode, the communication duration is set to $T_{\text{sum}} = 1000$ time slots, with each time slot lasting 1 ms. Since the position of user remains nearly fixed within 1 second, we assume that the user positions are fixed throughout each episode¹. The packet arrival rate for each user is set to $\lambda = 9.5$. Throughout this work, unless stated otherwise, identical arrival rates are assumed for all users, i.e.,

¹Note that, to accelerate the convergence of the algorithm, the user positions are randomly generated at each step within an episode during the training process.

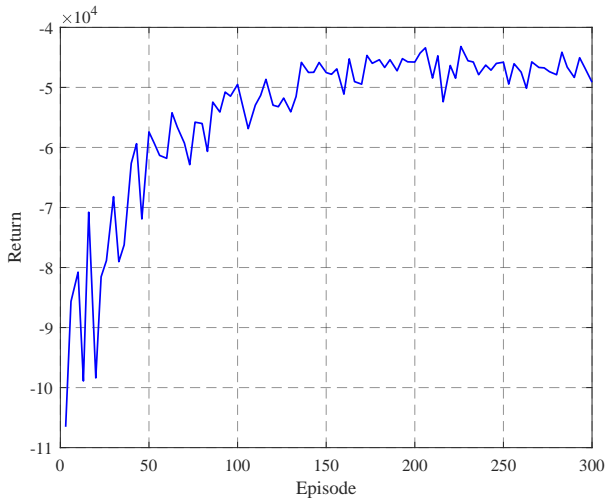


Fig. 5. Return for each training episode with increasing iterations.

$\lambda = \lambda_1 = \lambda_2 = \dots = \lambda_K$. The detailed hyperparameters are presented in Table I.

B. Baseline Methods

To reflect the performance of our proposed method, the following baseline methods are considered as follow.

- **Max sum rate:** The algorithm proposed in [34] and [35] are respectively employed for subcarrier allocation and RIS reflection shift optimization, while MRT is used for beamforming at the BS.
- **Max minimum rate:** This algorithm is the hybrid DRL algorithm with the reward to be $\min R_k[t]$ reward, as described in Section III-E, and it has not undergone transfer learning.
- **Random:** The RIS reflection shift and subcarrier allocation are set randomly. The active beamforming at BS is optimized using the MRT.
- **Without RIS:** This scheme represents a system that lacks RIS assistance, i.e., the number of RIS reflecting elements is set to $M = 0$.

C. Convergence and Validity Analysis

To validate the effectiveness and convergence of the proposed method, experiments are conducted. Fig. 5 shows the cumulative reward for each training episode. The figure demonstrates a progressive increase in the cumulative reward throughout the training process, indicating the effectiveness of our proposed method. Besides, the performance gradually stabilizes in around 150 training episodes, despite some fluctuations due to channel variations and changes of packets in buffers.

D. Latency Performance Analysis

Fig. 6 illustrates the average delay performance under varying packet arrival rates λ . The proposed algorithm consistently achieves the lowest average delay, demonstrating its superior

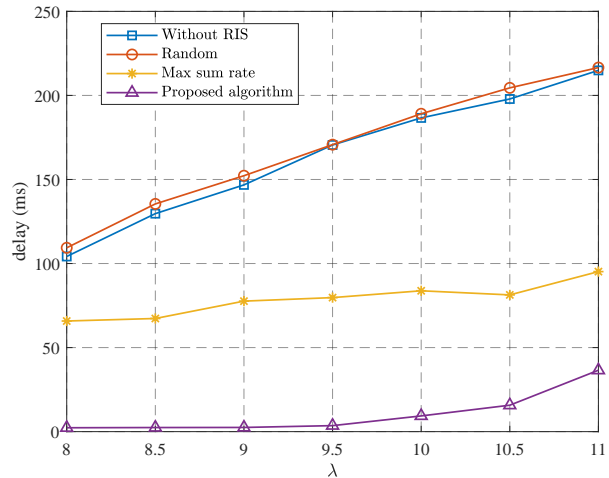


Fig. 6. Average delay performance under varying packet arrival rates λ .

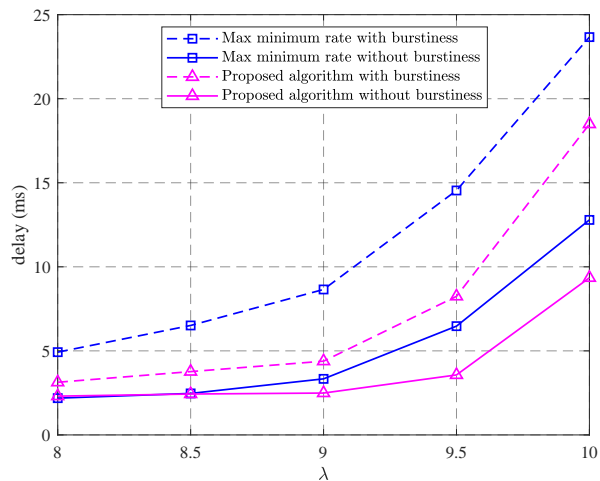
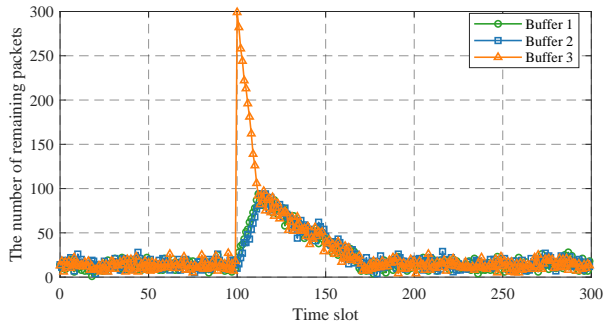


Fig. 7. Average delay performance as packet arrival rate λ varies.

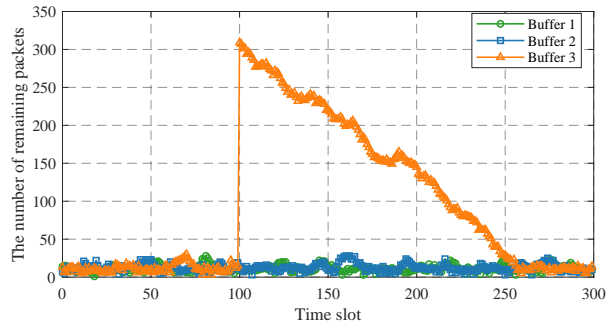
capability in minimizing latency. In contrast, the “without RIS” scheme results in the highest delay, emphasizing the critical role of RIS in improving delay performance. Although the “max sum rate” method performs better than baseline schemes such as “random” and “without RIS”, its overall delay performance is clearly inferior to that of the proposed method. This is because it prioritizes the maximization of system throughput without considering user fairness or queue stability, which leads to higher delays for certain users. The “random” method yields persistently high delays, further underlining the importance of intelligent and delay-aware resource allocation. Moreover, as the λ increases, the number of packets arriving at the buffer within each time slot grows accordingly, leading to aggravated buffer backlog and consequently resulting in an incremental increase in the average delay.

E. Latency Analysis in Burstiness Scenarios

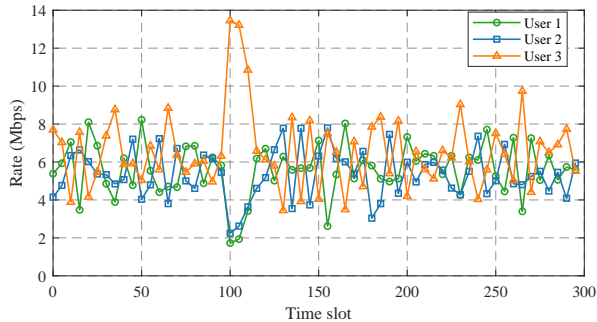
To evaluate the proposed algorithm under bursty traffic, we simulate sudden data arrivals by injecting 300 packets into



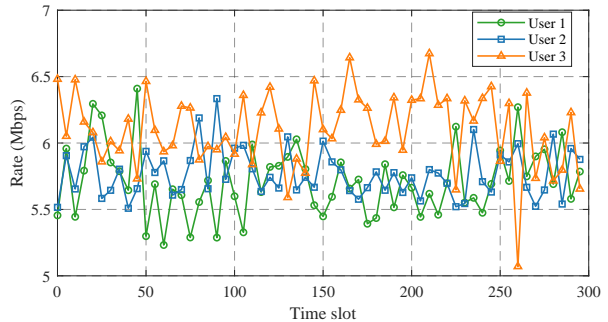
(a) The backlogged packets in each buffer of the proposed method.



(b) The backlogged packets in each buffer of the max minimum rate method.



(c) Transmission rates of the proposed method.



(d) Transmission rates of the max minimum rate method.

Fig. 8. The change of the backlogged packets and transmission rates in each buffer over time step of the proposed method and max minimum rate method in burstiness scenarios.

buffers 1, 2, and 3 at time slots 100, 400, and 700, respectively. Fig. 7 presents a comparison of the delay performance between the proposed algorithm and the “max minimum rate” algorithm under different scenarios. It can be observed that, regardless of whether burstiness is present, the proposed algorithm consistently demonstrates superior performance, effectively validating its effectiveness, in handling burstiness.

To further explain this advantage, we analyze a specific case by examining buffer backlogs and transmission rates during the first 300 time slots. As shown in Fig. 8(a), the proposed algorithm effectively reduces backlog by dynamically adjusting resource allocation in response to bursty arrivals. In contrast, Fig. 8(b) shows persistent congestion in buffer 3 under the “max minimum rate” approach, indicating inefficient allocation. Fig. 8(c) further shows that the proposed method prioritizes users with heavier backlogs, rapidly increasing their transmission rates, such as user 3, leading to quick backlog clearance. Conversely, Fig. 8(d) reveals that the baseline allocates resources more rigidly, ignoring buffer states and failing to relieve congestion effectively, which results in higher delay.

F. Impact of Reflection Elements M

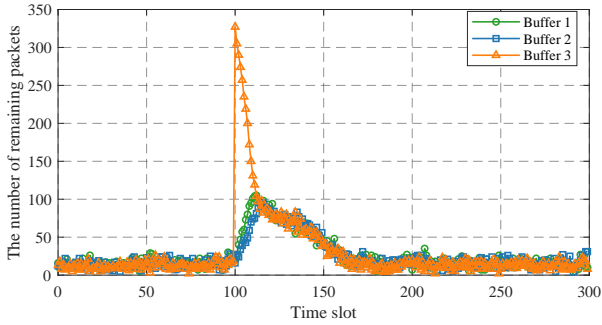
Fig. 10 illustrates the impact of the number of RIS reflection elements on the average delay performance under varying arrival rates λ . As observed, when $M = 36$, the average delay increases sharply once λ exceeds 9.0, suggesting that

the system struggles to accommodate high traffic loads. With $M = 64$, the delay grows more moderately but still experiences a considerable rise at elevated arrival rates. In contrast, when $M = 100$, the delay remains consistently low across all values of λ , demonstrating $M = 100$ is sufficient enough to support the considered service load with λ less than 10. This improvement is primarily attributed to the enhanced passive beamforming gain resulting from the increased number of RIS reflection elements, thereby improving the effective data rate. As a result, the system is able to accommodate higher traffic loads while maintaining low-latency communication performance.

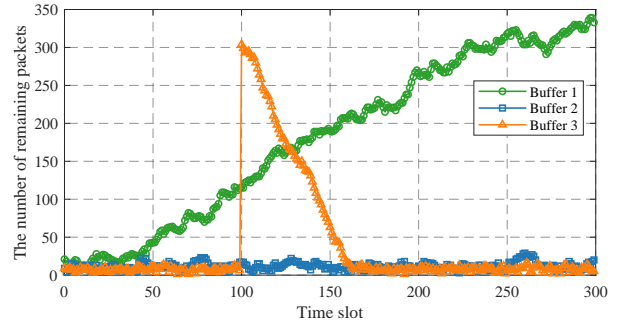
G. Latency Analysis under Different Traffic Flows

To evaluate the performance of the proposed algorithm under varying user arrival rates, we set the packet arrival rates $\lambda_1 = \lambda + \text{gap}$, $\lambda_2 = \lambda$, and $\lambda_3 = \lambda - \text{gap}$. As shown in Fig. 11, the delay of the “max minimum rate” method increases with larger gaps, while the proposed algorithm maintains consistently low delay, indicating strong robustness even when trained under uniform arrival rates.

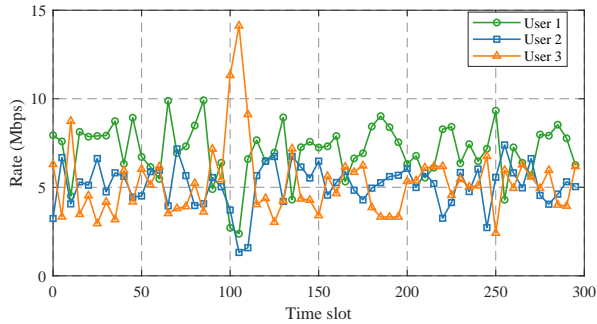
To further explain this advantage, we analyze a specific case by examining buffer backlogs and transmission rates during the first 300 time slots. In Fig. 9(a), the proposed algorithm keeps buffer backlogs balanced despite differing arrival rates, showing its fairness. Upon the burst at time slot 100, it quickly reallocates resources to clear buffer 3. In contrast, Fig. 9(b)



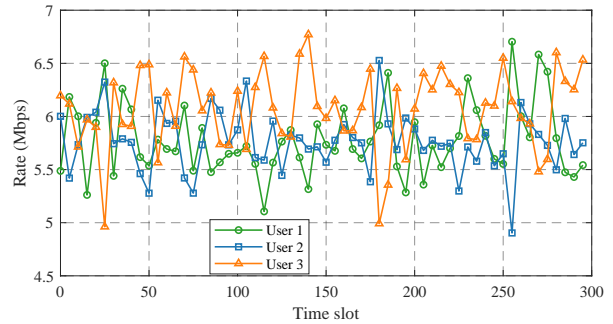
(a) The backlogged packets in each buffer of the proposed method.



(b) The backlogged packets in each buffer of the max minimum rate method.



(c) Transmission rates of the proposed method.



(d) Transmission rates of the max minimum rate method.

Fig. 9. The change of the backlogged packets and transmission rates in each buffer over time step of the proposed method and max minimum rate method in different traffic flows scenarios.

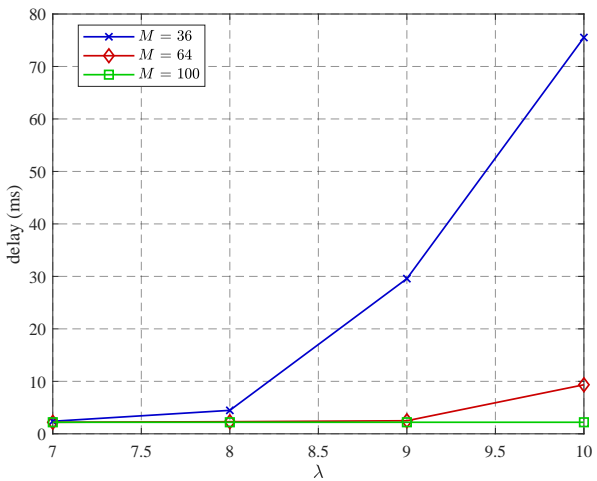


Fig. 10. Impact of reflection elements M on delay performance.

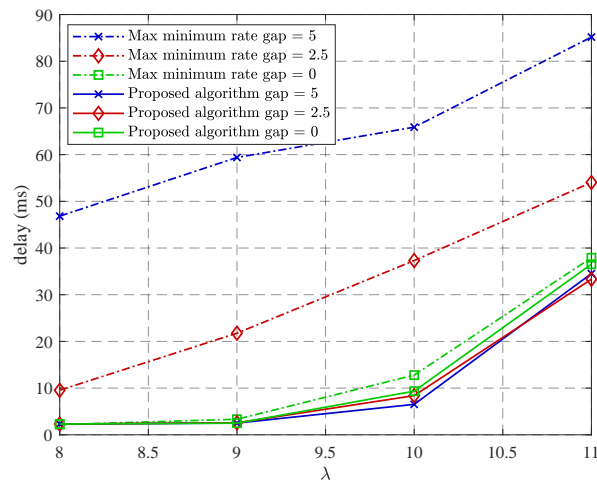


Fig. 11. Average delay performance as distinct packet arrival rate λ varies.

shows the “max minimum rate” approach leads to severe congestion in buffer 1 due to static rate-based allocation. Further, Fig. 9(c) reveals the proposed method allocates more resources to high arrival rate users and dynamically adapts to queue states. Before time slot 100, user 3 has a lower rate due to low arrival, but receives rapid support when the burst occurs. Conversely, Fig. 9(d) shows that the “max minimum rate” method rigidly enforces rate fairness, ignoring buffer states,

resulting in inefficient resource use and longer delays.

H. Jitter Analysis

To evaluate the jitter performance of our proposed algorithm, we conduct measurements and analysis based on the

TABLE II
THE ROBUSTNESS OF PROPOSED APPROACH ON AVERAGE DELAY.

Algorithm	Delay taps ($L_0 = 6, L_1 = 3, L_3 = 4$)	Distribution ($R = 15$ m, $D_3 = 3$ m)	Rician factor ($k_{BR} = 3$ dB, $k_{RU} = 4$ dB)
Proposed algorithm	9.6902 ms	63.3849 ms	6.2181 ms
Max sum rate	91.1677 ms	72.8252 ms	78.7498 ms
Max minimum rate	27.3113 ms	64.5808 ms	9.4219 ms
Random	167.4868. ms	207.0432 ms	174.2089 ms

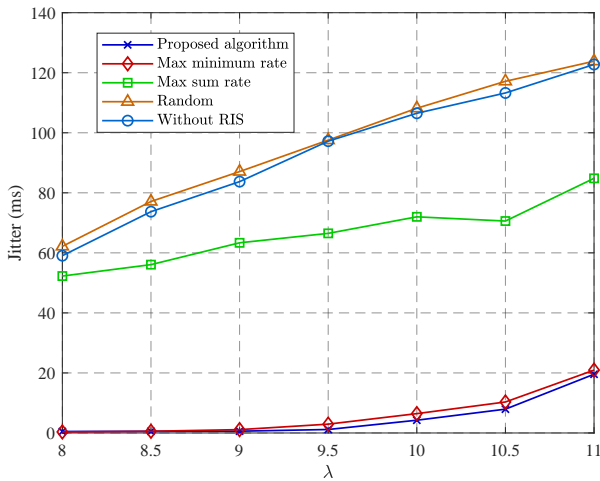


Fig. 12. Jitter performance as arrival rate λ varies.

jitter definition provided in [36], as given by

$$\frac{1}{K} \sum_{k=1}^K \sqrt{\frac{1}{m(k)} \sum_{g=1}^{m(k)} \left(T_D^{(k)}(g) - \frac{1}{m(k)} \sum_{g=1}^{m(k)} T_D^{(k)}(g) \right)^2}, \quad (27)$$

As illustrated in Fig. 12, the proposed algorithm consistently achieves the lowest jitter across all values of λ , demonstrating its superior capability in balancing resource allocation and maintaining latency stability. In contrast, the “max-min rate” scheme yields slightly higher jitter, while the “max sum rate” approach, although effective in optimizing overall throughput, results in significantly increased jitter. The “random” allocation and “without RIS” schemes exhibit the worst jitter performance, underscoring the effectiveness of both learning-based optimization and RIS assistance in enhancing system delay stability. Moreover, as the arrival rate λ increases, jitter also exhibits a rising trend, indicating that the system becomes increasingly unstable under higher traffic loads and struggles to maintain consistent delay performance.

I. Robustness Validation

Table II presents a robustness evaluation of the proposed algorithm in terms of average delay under three distinct transmission scenarios: varying delay taps ($L_0 = 6, L_1 = 3, L_3 = 4$), spatial distribution parameters ($R = 15$ m, $D_3 = 3$ m), and Rician fading factors ($k_{BR} = 3$ dB, $k_{RU} = 4$ dB). The per-user arrival rate is fixed at $\lambda = 9.5$, with all other

parameters following the baseline in Section IV-A. Across all scenarios, the proposed algorithm consistently achieves the lowest delay, significantly outperforming benchmark methods. In contrast, the “max sum rate” approach leads to notably higher delays, while the “max minimum rate” shows moderate performance. The “random” strategy results in the worst delay across all settings. These results confirm the strong adaptability and delay minimization capability of the proposed algorithm under diverse transmission conditions. Its robustness against variations in different delay taps, user distribution, and fading characteristics highlights its potential for real-world deployment in dynamic wireless environments.

V. CONCLUSION

This paper introduced a novel DRL-based approach to minimize the average delay while ensuring user fairness in different traffic flows. Unlike traditional methods, our proposed solution extends the state information to encompass a comprehensive set of factors, including channel state information, the number of backlogged packets in buffer and the number of current arrival packets. To address the challenges posed by the hybrid action space, we develop a hybrid DRL framework, where the action space consists of both continuous and discrete components. Specifically, PPO- Θ is employed to optimize the continuous RIS reflection phase shifts, while PPO- N is designed to handle the discrete subcarrier allocation decisions. Furthermore, to tackle the curse of dimensionality arising from multi-dimensional discrete variables, we introduced a multi-agent strategy to optimize subcarrier allocation decisions efficiently. Through extensive numerical evaluations, our method demonstrated significant improvements in reducing the average delay while maintaining user fairness, surpassing existing baseline methods. Additionally, the results highlighted the superior stability and adaptability of our approach. This work provides a robust and scalable solution to the delay optimization in RIS-assisted OFDM systems, leveraging advanced machine learning techniques to optimize resource allocation in next-generation wireless networks, paving the way for more efficient and equitable network management.

REFERENCES

- [1] C.-X. Wang *et al.*, “On the road to 6G: Visions, requirements, key technologies, and testbeds,” *IEEE Commun. Surv. Tutorials*, vol. 25, no. 2, pp. 905–974, Secondquarter 2023.
- [2] Z. Zhang *et al.*, “6G wireless networks: Vision, requirements, architecture, and key technologies,” *IEEE Veh. Technol. Mag.*, vol. 14, no. 3, pp. 28–41, Sep. 2019.

- [3] E. Basar, M. Di Renzo, J. De Rosny, M. Debbah, M.-S. Alouini, and R. Zhang, "Wireless communications through reconfigurable intelligent surfaces," *IEEE Access*, vol. 7, pp. 116 753–116 773, 2019.
- [4] Z. Ma, M. Xiao, Y. Xiao, Z. Pang, H. V. Poor, and B. Vucetic, "High-reliability and low-latency wireless communication for internet of things: Challenges, fundamentals, and enabling technologies," *IEEE Internet Things J.*, vol. 6, no. 5, pp. 7946–7970, Oct. 2019.
- [5] W. Jiang, B. Han, M. A. Habibi, and H. D. Schotten, "The road towards 6G: A comprehensive survey," *IEEE open j. Commun. Soc.*, vol. 2, pp. 334–366, Feb. 2021.
- [6] M. Waqas *et al.*, "A comprehensive survey on mobility-aware D2D communications: Principles, practice and challenges," *IEEE Commun. Surveys Tuts.*, vol. 22, no. 3, pp. 1863–1886, thirdquarter 2020.
- [7] J. Liu, W. Chen, and K. B. Letaief, "Delay optimal scheduling for ARQ-aided power-constrained packet transmission over multi-state fading channels," *IEEE Trans. Wireless Commun.*, 2017.
- [8] Y. Liu *et al.*, "Reconfigurable intelligent surfaces: Principles and opportunities," *IEEE Commun. Surv. Tutorials*, vol. 23, no. 3, pp. 1546–1577, thirdquarter 2021.
- [9] M. Bennis, M. Debbah, and H. V. Poor, "Ultrareliable and low-latency wireless communication: Tail, risk, and scale," *Proc. IEEE*, vol. 106, no. 10, pp. 1834–1853, Oct. 2018.
- [10] G. Yang, M. Xiao, and H. V. Poor, "Low-latency millimeter-wave communications: Traffic dispersion or network densification?" *IEEE Trans. Commun.*, vol. 66, no. 8, pp. 3526–3539, Aug. 2018.
- [11] C. Guo, L. Liang, and G. Y. Li, "Resource allocation for low-latency vehicular communications: An effective capacity perspective," *IEEE J. Sel. Areas Commun.*, vol. 37, no. 4, pp. 905–917, Apr. 2019.
- [12] L. Liang, G. Y. Li, and W. Xu, "Resource allocation for D2D-enabled vehicular communications," *IEEE Trans. Commun.*, vol. 65, no. 7, pp. 3186–3197, Jul. 2017.
- [13] O. L. Alcaraz López, H. Alves, and M. Latva-aho, "Joint power control and rate allocation enabling ultra-reliability and energy efficiency in SIMO wireless networks," *IEEE Trans. Commun.*, vol. 67, no. 8, pp. 5768–5782, Aug. 2019.
- [14] W. Sun, E. G. Ström, F. Brännström, Y. Sui, and K. C. Sou, "D2D-based V2V communications with latency and reliability constraints," in *Proc. IEEE Globecom Workshops*, 2014, pp. 1414–1419.
- [15] Y. Guo, Q. Yang, J. Liu, and K. S. Kwak, "Cross-layer rate control and resource allocation in spectrum-sharing ofdma small-cell networks with delay constraints," *IEEE Trans. Veh. Technol.*, vol. 66, no. 5, pp. 4133–4147, May 2017.
- [16] J. Su, Z. Liu, Y.-a. Xie, K. Y. Chan, and X. Guan, "Dynamic resource allocation in queue-constrained and delay-sensitive vehicular networks," *IEEE Trans. Intell. Veh.*, vol. 8, no. 10, pp. 4434–4444, Oct. 2023.
- [17] J. Su *et al.*, "Semantic communication-based dynamic resource allocation in d2d vehicular networks," *IEEE Trans. Veh. Technol.*, vol. 72, no. 8, pp. 10 784–10 796, Aug. 2023.
- [18] H. Yu, M. H. Cheung, L. Huang, and J. Huang, "Power-delay tradeoff with predictive scheduling in integrated cellular and Wi-Fi networks," *IEEE J. Sel. Areas Commun.*, vol. 34, no. 4, pp. 735–742, 2016.
- [19] Z. Qin, G. Y. Li, and H. Ye, "Federated learning and wireless communications," *IEEE Wireless Commun. Lett.*, vol. 28, no. 5, pp. 134–140, Oct. 2021.
- [20] Y. Zhao, Y. Kim, and J. Lee, "SOQ: Structural reinforcement learning for constrained delay minimization with channel state information," *IEEE Internet of Things Journal*, vol. 11, no. 3, pp. 4628–4644, Feb. 2024.
- [21] L. Liang, H. Ye, and G. Y. Li, "Spectrum sharing in vehicular networks based on multi-agent reinforcement learning," *IEEE J. Sel. Areas Commun.*, vol. 37, no. 10, pp. 2282–2292, Oct. 2019.
- [22] J. Sang *et al.*, "Coverage enhancement by deploying RIS in 5G commercial mobile networks: Field trials," *IEEE Wirel. Commun.*, vol. 31, no. 1, pp. 172–180, Feb. 2024.
- [23] Y. Xu, Z. Gao, Z. Wang, C. Huang, Z. Yang, and C. Yuen, "RIS-enhanced WPCNs: Joint radio resource allocation and passive beamforming optimization," *IEEE Trans. Veh. Technol.*, vol. 70, no. 8, pp. 7980–7991, Aug. 2021.
- [24] G. Zhou, C. Pan, H. Ren, K. Wang, and Z. Peng, "Secure wireless communication in RIS-aided MISO system with hardware impairments," *IEEE Wireless Commun. Lett.*, vol. 10, no. 6, pp. 1309–1313, Jun. 2021.
- [25] H. Guo, Y.-C. Liang, J. Chen, and E. G. Larsson, "Weighted sum-rate maximization for reconfigurable intelligent surface aided wireless networks," *IEEE Trans. Wireless Commun.*, vol. 19, no. 5, pp. 3064–3076, May 2020.
- [26] C. Huang, A. Zappone, G. C. Alexandropoulos, M. Debbah, and C. Yuen, "Reconfigurable intelligent surfaces for energy efficiency in wireless communication," *IEEE Trans. Wireless Commun.*, vol. 18, no. 8, pp. 4157–4170, Aug. 2019.
- [27] Z. Yang, L. Xia, J. Cui, Z. Dong, and Z. Ding, "Delay and energy minimization for cooperative NOMA-MEC networks with SWIPT aided by RIS," *IEEE Trans. Veh. Technol.*, vol. 73, no. 4, pp. 5321–5334, Aug. 2024.
- [28] S. Jiang, X. Wang, J. Lin, C. Huang, Z. Qian, and Z. Han, "A delay-oriented joint optimization approach for RIS-assisted MEC-MIMO system," *IEEE Trans. Mob.*, pp. 1–15, Dec. 2024.
- [29] T. Bai, C. Pan, Y. Deng, M. Elkhshlan, A. Nallanathan, and L. Hanzo, "Latency minimization for intelligent reflecting surface aided mobile edge computing," *IEEE J. Sel. Areas Commun.*, vol. 38, no. 11, pp. 2666–2682, Nov. 2020.
- [30] N. Zhang, Y. Liu, X. Mu, W. Wang, and A. Huang, "Queue-aware STAR-RIS assisted NOMA communication systems," *IEEE Trans. Wireless Commun.*, vol. 23, no. 5, pp. 4786–4801, May 2024.
- [31] J. Jia, K. Yu, X. Mu, Y. Liu, J. Chen, and X. Wang, "Delay-aware resource allocation for RIS assisted semi-grant-free NOMA systems," *IEEE Trans. Commun.*, vol. 73, no. 3, pp. 2016–2031, Mar. 2025.
- [32] D. Kakadia, J. Yang, A. Gilgur, D. Kakadia, J. Yang, and A. Gilgur, "Evolved universal terrestrial radio access network (EUTRAN)," *Network performance and fault analytics for LTE wireless service providers*, pp. 61–81, 2017.
- [33] H. Fang *et al.*, "Power allocation for delay optimization in device-to-device networks: A graph reinforcement learning approach," *IEEE Trans. Veh. Technol.*, early access 2025.
- [34] Y. Yang, S. Zhang, and R. Zhang, "IRS-enhanced OFDMA: Joint resource allocation and passive beamforming optimization," *IEEE Wireless Commun. Lett.*, vol. 9, no. 6, pp. 760–764, Jun. 2020.
- [35] Y. Yang, B. Zheng, S. Zhang, and R. Zhang, "Intelligent reflecting surface meets OFDM: Protocol design and rate maximization," *IEEE Trans. Commun.*, vol. 68, no. 7, pp. 4522–4535, Jul. 2020.
- [36] C. Zhang, L. Wei, J. Fan, Z. Liu, and Y. Huang, "Lyapunov-guided multi-agent reinforcement learning for delay-sensitive wireless scheduling," *arXiv preprint arXiv:2411.01766*, 2024.